Ultrasound in Med. & Biol., Vol. 00, No. 00, pp. 1–12, 2021

0301-5629/$ - see front matter

https://doi.org/10.1016/j.ultrasmedbio.2021.12.001

● *Original Contribution*

MYOCARDIAL STRAIN IMAGING WITH ELECTROCARDIOGRAM-GATED AND COHERENT COMPOUNDING FOR EARLY DIAGNOSIS OF CORONARY ARTERY DISEASE

JULIEN GRONDIN,* CHANGHEE LEE,† RACHEL WEBER,† and ELISA E. KONOFAGOU*,†

* Department of Radiology, Columbia University, New York, New York, USA; and † Department of Biomedical Engineering, Columbia University, New York, New York, USA

(*Received* 14 *June* 2021; *revised* 22 *November* 2021; *in final form* 1 *December* 2021)

Abstract—Myocardial elastography (ME) is an ultrasound-based technique that uses radiofrequency signals for 2-D cardiac motion tracking and strain imaging at a high frame rate. Early diagnosis of coronary artery disease (CAD) is critical for timely treatment and improvement of patient outcome. The objective of this study was to assess the performance of ME radial and circumferential strains in the detection and characterization of CAD in patients. In this study, 86 patients suspected of CAD were imaged with ME prior to invasive coronary angiography (ICA). End-systolic radial and circumferential left ventricular strains were estimated in all patients in each of their perfusion territories: left anterior descending (LAD), left circumflex (LCX) and right coronary artery (RCA). ME radial strains were capable of differentiating the obstructive CAD group (55.3 ± 29.8%) from the non-obstructive CAD (72.5 ± 46.8%, $p < 0.05$) and no CAD groups (73.4 ± 30.4%, $p < 0.05$) in the RCA territory. ME circumferential strains were capable of differentiating the obstructive CAD group (−3.1 ± 7.5%) from the non-obstructive CAD (−7.2 ± 6.8%, $p < 0.05$) and normal (−6.9 ± 8.0%, $p < 0.05$) groups in the LAD territory and to differentiate the normal group (−17.1 ± 8.2%) from the obstructive (−12.8 ± 7.2%, $p < 0.05$) and non-obstructive CAD (−13.6 ± 8.5%, $p < 0.05$) groups in the RCA territory. ME circumferential strain performed better than ME radial strain in differentiating normal, non-obstructive and obstructive perfusion territories. In the LCX territory, both ME radial and circumferential strains decreased when the level of stenosis was higher. However, it was not statistically significant. The findings presented herein indicate that ME radial and circumferential estimation obtained from ECG-gated and compounded acquisitions is a promising tool for early, non-invasive and radiation-free detection of CAD in patients. (E-mail:)

Key Words: **Cardiac strain imaging, Electrocardiogram-gated, Coherent compounding, Coronary artery disease, Coronary angiography.**

INTRODUCTION

Coronary artery disease (CAD) is the leading cause of death in the world with 8.9 million deaths in 2017 and affects 18.2 million adults in the United States (Virani et al. 2020). Various methods are used to detect ischemia, such as exercise electrocardiogram (ECG), stress echocardiography, single-photon emission computed tomography, positron emission tomography and cardiac magnetic resonance, or to assess coronary anatomy, such as coronary computed tomography angiography and magnetic resonance coronary angiography (Montalescot et al. 2013). Stress echocardiography is ultrasound based and has the advantages of portability, low risk and high temporal resolution. However, it requires the patient to be stressed either by exercising or pharmacologically, and is based on a visual assessment of wall motion abnormalities, which is subjective.

Strain imaging can distinguish tissue motion with deformation from tissue motion without significant deformation. Several studies have reported that strain at rest is sensitive to the presence and severity of coronary stenosis (Choi et al. 2009; Tsai et al. 2010; Shimoni et al. 2011; Montgomery et al. 2012; Biering-Sorensen et al. 2014). Cardiac strain imaging was reported to have higher discriminative power than visual assessment of wall motion abnormalities in the detection of coronary stenosis (Stankovic et al. 2015). Cardiac strain can be obtained with speckle tracking

Address correspondence to: Elisa E. Konofagou, 630 West 168th Street, P&S 19-418, New York, NY 10032, USA E-mail: ek2191@columbia.edu

echocardiography (Amzulescu et al. 2019) using B-mode images, which are based on the envelope of the ultrasound radiofrequency (RF) signals. However, previous studies have found that tracking of RF signals provides better performance than envelope signals for tissue deformation estimation (Alam and Ophir 1997; Ma and Varghese 2013). Myocardial elastography (ME) is an ultrasound technique for myocardial strain imaging using RF signals acquired at high frame rates (Konofagou et al. 2002; Lee et al. 2007; Zervantonakis et al. 2007). The use of RF signals to derive myocardial strains at conventional frame rates (38−50 frames/s) has also been reported (Varghese et al. 2003; Behar et al. 2004). Several techniques can be used for high-frame-rate cardiac ultrasound imaging (Cikes et al. 2014). In this study, we focused on ECG-gated acquisitions, which assemble small sectors of RF signals acquired at different heartbeats into a full echocardiographic view (Wang et al. 2008), and diverging (unfocused) wave emission (Hasegawa and Kanai 2011; Provost et al. 2011; Sayseng et al. 2020). ECG-gated acquisitions can take approximately 7 s to ensure having at least one heartbeat per sector; it can lead to sector alignment artifacts in patients unable to hold their breath during the entire acquisition. On the other hand, diverging wave acquisitions can be performed in 2 s, as an alternative. In a previous *in vivo* study, we reported that ECG-gated acquisitions yield slightly more precise left ventricular (LV) radial strains than compounded acquisitions (Sayseng et al. 2020). ME has been validated against tagged magnetic resonance imaging and was found capable of differentiating normal from reperfused myocardium (Lee et al. 2008). ME has also been found capable of detecting, identifying and characterizing as small as a 40% blood flow reduction in the left anterior descending artery (LAD) in an acute ischemia canine model *in vivo* (Lee et al. 2011). End-systolic radial strains were found to decrease from approximately 28% (at baseline) to −3% (after 40% blood flow reduction) in the anterior region. More recently, ME has been reported to yield reproducible LV radial strains in consecutive acquisitions and yield lower end-systolic LV radial strains in ischemic than in normal patients with single diverging wave imaging (Grondin et al. 2017a). Use of coherent compounding of diverging waves to image the heart has been reported to provide better image quality and strain estimates than single diverging waves (Grondin et al. 2017b). ME in the short-axis view offers the advantage of evaluating all three coronary perfusion territories in the same acquisition.

In this study, the performance of ME strains with either ECG-gated or compounding acquisitions to detect CAD was investigated. Because ECG-gated acquisitions were found to provide slightly more precise strain estimates than compounded acquisitions in prior studies (Sayseng et al. 2020), ECG-gated was used as the preferred method of acquisition. However, ECG-gated acquisitions have a long duration to ensure that at least one heart cycle is captured for each acquisition sector. Therefore, if a patient breathes during the acquisition, there can be significant motion artifacts preventing co-registration of the sectors. In this study, ECG-gated acquisitions were performed only in patients able to hold their breath for a sufficient duration (7 s) to avoid respiratory motion artifacts; otherwise, compounded acquisitions were performed. Both the radial and circumferential components of ME strains were evaluated. It is also important to be able to distinguish patients with non-obstructive CAD (10%−49% stenosis) from patients with normal epicardial vessel, as the incidence of all-cause death and non-fatal myocardial infarction (MI) was found to be 2.5 times higher in the former than in the latter group (Radico et al. 2018). In addition, a rate of 66% of patients with acute myocardial infarction with less than 50% coronary stenosis on their angiogram has been reported. The objective of this study was to investigate the performance of ME-based radial and circumferential strain with ECG-gated and compounding acquisitions to differentiate normal, non-obstructive and obstructive CAD (≥50%) patients and perfusion territories.

METHODS

Study population

In this study, patients scheduled for an invasive coronary angiography were screened. Patients with prior known myocardial infarct, stent, bypass surgery and heart transplants were excluded from the study. Of the 180 total number of patients meeting the inclusion criteria and recruited for this study, 94 were excluded because of poor B-mode (75/94) or tracking quality (19/94) (Table 1). B-Mode and tracking quality were manually classified using a binary rating system. Poor B-mode quality was defined as the inability to visualize the endocardial border. Poor tracking quality was defined as a misalignment between the motion of the actual and that of the tracked endocardial border during systole. The study protocol was approved by an institutional review board (IRB) of Columbia University, and informed consent was obtained before the study.

Table 1. Number of patients excluded because of poor B-mode and tracking quality

	Poor B-mode quality	Poor tracking quality	Total
Compounding	40	12	52
Electrocardiogram-gated	35	7	42

Myocardial elastography

The patients were imaged with customized ultrasound sequences prior to and on the same day as coronary angiography. None of the patients received any sedation prior to the ultrasound scan. The heart was imaged in short-axis view at the basal, mid- and apical levels. A 2.5-MHz center frequency transducer (P4-2, ATL/Philips, Andover, MA, USA) connected to a research ultrasound scanner (Vantage 256, Verasonics, Kirkland, WA, USA) was used to scan the patients. The ECG signal was acquired synchronously with the ultrasound data using an ECG unit (IX-BIO4, iWorx, Dover, NH, USA) triggered by the ultrasound scanner. Two different high-frame-rate imaging sequences were used to acquire ultrasound signals: coherent compounding of diverging waves and ECG-gated focused transmissions, which have been previously described (Sayseng et al. 2020). Briefly, diverging wave imaging was performed with 10 virtual sources placed 10 mm behind the surface of the transducer and transmitting at different angles from -15° to 15° at a pulse repetition frequency (PRF) of 3 kHz over 2 s, yielding a compounded frame rate of 300 frames/s. On the other hand, ECG-gated acquisitions were performed using five sectors, with 16 transmit beams per sector at a pulse repetition frequency (PRF) of 3200 Hz, a focal depth of 8 cm and 1.4-s acquisition duration per sector, yielding an imaging frame rate of 200 frames/s. For patients who were not able to perform breathholding for the entire duration of the ECG-gated acquisition (7 s), coherent compounding acquisition was performed because of possible motion artifacts. Therefore, ECG-gated and compounding acquisitions were performed alternatively, depending on the patient. For both acquisition methods, the imaging field of view was 90°. The RF channel data were acquired on the 64 elements of the probe and sampled at four samples per wavelength. A standard delay-and-sum method was used to reconstruct the ultrasound images for both transmit methods (Grondin et al. 2015; Sayseng et al. 2018). Axial motion estimation was performed at the same rate as the imaging rate (300 Hz for compounding and 200 Hz for ECG-gated acquisitions), while lateral motion estimation was performed at 100 Hz after temporal downsampling for improved lateral motion estimation (Sayseng et al. 2018). Because lateral sampling is coarser (180 lines over 90°, *i.e.,* 0.70 mm/sample at a depth of 80 mm) than axial sampling (2078 samples over 160 mm, *i.e.,* 0.077 mm/sample), if the motion estimation rate is too high, there may not be sufficient lateral motion between the reference and comparison frames, which can lead to inaccurate lateral motion estimation (Sayseng et al. 2018). Lateral displacements estimated at 100 Hz were subsequently upsampled back to the original frame rate (300 Hz for compounding and 200 Hz for ECG-gated acquisitions) to match the axial motion estimation rate. A linear temporal interpolation was used for this upsampling process. Motion estimation was performed using normalized 1-D (axial) cross-correlation (Luo and Konofagou 2010) in a 2-D (axial and lateral) search (Konofagou and Ophir 1998) with a window length of 5.9 mm (=9.6 wavelengths) and 90% overlap. The window length was selected based on prior studies (Chen et al. 2007; Lee et al. 2008) that found a window length of approximately 10 wavelengths yielded less noisy displacement and more precise strain estimates. The lateral search range was 1 beam with a 10:1 linear interpolation factor. The axial and lateral displacements were accumulated during mechanical systole only, defined from the axial displacement M-mode during the inward motion (Grondin et al. 2017a). More specifically, to manually select the systolic phase, the axial displacement M-mode was obtained along the line through the center of the ultrasound array and the center of the left ventricular cavity. The axial displacement M-mode and the ECG were displayed over a duration of 400 ms starting from the ECG R wave. The onset of systole was defined as the first time point for which the anterior wall exhibited a downward motion and the inferior wall exhibited an upward motion. End systole was defined as the time point at which there was no longer an inward motion. Manual selection of systole could be adjusted by visualizing the B-mode movie during the selected time window and ensuring that the entire LV inward motion was included. For each pixel, appropriate registration between consecutive displacement images was performed to ensure that the cumulative displacement depicted the motion of the same tissue region. The axial and lateral displacements were scan-converted from polar to Cartesian coordinates and median filtered with a 5×5-mm kernel. The 2-D (axial and lateral) Lagrangian strain tensor $\mathbf{E}$ was derived using a least-squares estimator implemented with Savitzky–Golay filters (Luo et al. 2004), where $\mathbf{E}$ is defined as

$$\mathbf{E} = \frac{1}{2}\left(\nabla \mathbf{u} + (\nabla \mathbf{u})^T + (\nabla \mathbf{u})^T \nabla \mathbf{u} \right)$$

where $\nabla \mathbf{u}$ is the 2-D displacement gradient tensor defined by

$$\nabla \mathbf{u} = \begin{bmatrix} \frac{\partial u_x}{\partial x} & \frac{\partial u_x}{\partial y} \\ \frac{\partial u_y}{\partial x} & \frac{\partial u_y}{\partial y} \end{bmatrix}$$

where $\mathbf{u}$ is the 2-D displacement vector.

The endocardial and epicardial borders were manually segmented by an operator blinded to the angiography results. The radial strains were then derived from the 2-D strain tensor with the origin of the polar

coordinate system at the centroid of the segmented myocardium (Lee et al. 2007). The myocardium was divided into four (at the apical level) or six (at the basal and midcavity levels) sectors in accordance with the American Heart Association 17-segment model (Voigt et al., 2015), with equal sector angles. The end-systolic radial strains were averaged in each myocardial segment. Circumferential strain estimation was performed using a point-tracking method, described below, versus the generally used least-squares method, as the least-squares method did not provide sufficiently accurate transmural circumferential strain estimates. Tracking points were positioned along the endocardial border of each myocardial segment at end diastole (Fig. 1). The coordinates (x, y) of the tracking points for a given frame number n during systole were obtained using

$$x(n) = x(n=0) + \sum_{(f=1)}^{n} dX(x(f-1), y(f-1), f), \text{ for } n \geq 1$$

$$y(n) = y(n=0) + \sum_{(f=1)}^{n} dY(x(f-1), y(f-1), f), \text{ for } n \geq 1$$

where $x(n=0)$ and $y(n=0)$ are the axial and lateral coordinates of the tracking points at end diastole, and dX and dY are the interframe axial and lateral displacements, respectively, obtained from RF-based motion estimation. For each myocardial segment, the mean distance $R(t)$ between the myocardium centroid and the tracking points was calculated over the entire systolic phase. The arc length of the endocardial border of each segment

$L(n)$ was calculated as

$$L(n) = R(n)\theta$$

where $\theta = 2\pi/N$ is the angle of each myocardial sector, assumed to be constant during systole, and N is the number of sectors in the short-axis level. The endocardial circumferential Lagrangian strains $\varepsilon_c(n)$ were calculated from the tracking points in each myocardial segment as $\varepsilon_c(n) = \Big(L(n) - L(n=0)\Big) / \Big(L(n=0)\Big)$. In addition to circumferential strain calculation, endocardial tracking also allowed for manually classifying the tracking quality as correct or incorrect by a trained operator. Acquisition views with insufficient B-mode and tracking quality were discarded from the analysis. The radial and circumferential strains were obtained from axial strains estimated at the original frame rate and from lateral strains upsampled to the original frame rate after estimation at 100 Hz.

Territory selection

The left ventricle was divided into three major coronary vascular territories assuming the most common right heart dominance for all patients (Voigt et al. 2015). The LAD perfuses the anterior and anteroseptal at the basal and midcavity levels, as well as the apical anterior and septal regions; the LCX perfuses the inferolateral and anterolateral at the basal and midcavity levels as well as apical lateral regions; and the RCA perfuses the inferoseptal and inferior at the basal and midcavity levels

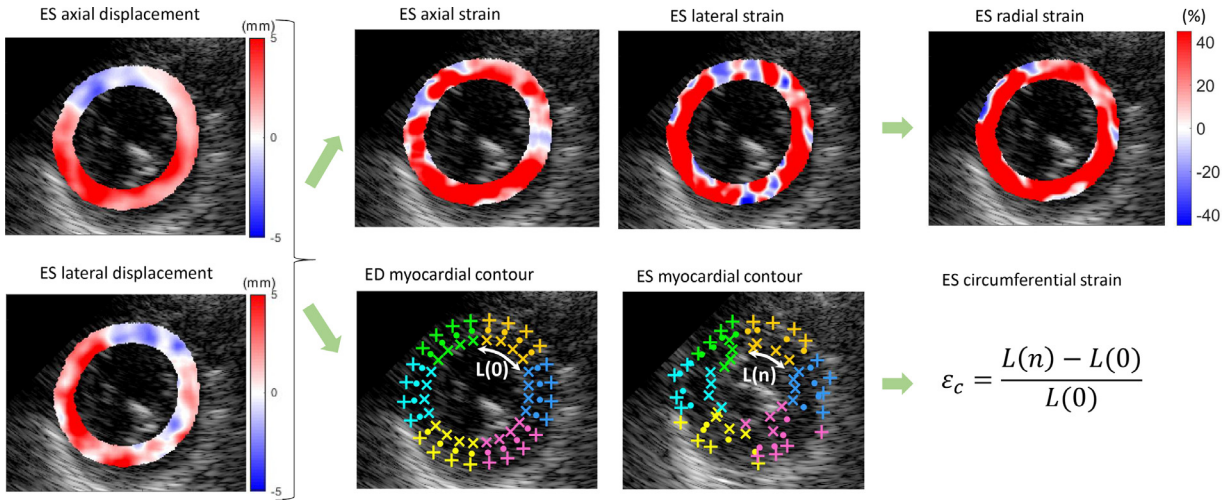

Fig. 1. Flowchart for the derivation of radial and circumferential strain from axial and lateral displacements in a normal patient. Axial and lateral strains are calculated and converted into radial strains. The epicardial and endocardial contours are delineated, and the myocardium is divided into six segments (or four segments for at the apical level). The myocardial contour is tracked throughout systole. For each segment, the circumferential strain (ε_c) is calculated as the relative change in endocardial contour from ED to ES. ED = end diastole; ES = end systole.

as well as apical inferior regions. The end-systolic radial and cirumferential strains were averaged in each of the three territories across short-axis levels.

Coronary angiography

The patients were escorted to the procedure room, and left and right coronary angiography was performed by advancing a catheter to the aorta and positioning it in the ostium of the left main and the right coronary arteries, respectively. Angiography was performed in multiple projections. Omnipaque and Visipaque (GE Healthcare, Chicago, IL, USA) were used as a contrast agent. All images were assessed by a cardiology board-certified physician. Epicardial vessels with ≥50% stenosis on the angiogram were considered obstructive, whereas those with 10%−49% stenosis were considered non-obstructive and coronaries with no stenosis were considered normal.

Clinical echocardiography

The presence of wall motion abnormalities (WMAs) in patients who had received an echocardiographic evaluation as part of their clinical standard of care was taken into account. The capability of WMAs to detect CAD was compared with the ME performance.

Statistical analysis

All statistical analyses were performed using GraphPad Prism 9 (GraphPad Software, San Diego, CA, USA). A χ^2-test for categorical variables and an analysis of variance (ANOVA) test for continuous variables were used to investigate if the distribution of patient characteristics in Table 2 differed. The mean and standard deviation of end-systolic radial and circumferential strains in each perfusion territory were computed for normal, non-obstructive and obstructive CAD coronary arteries. A one-way ANOVA with multiple comparison and Holm−Šídák correction was used to compare the end-systolic mean strains between the normal, non-obstructive and obstructive coronary arteries for each territory and with all territories combined.

RESULTS

Among all the included patients, 21 were found to be normal, 28 had non-obstructive CAD and 37 patients had obstructive CAD. Twenty patients were found to have obstructive single-vessel CAD, 11 patients were found to have obstructive double-vessel CAD and 6 patients were found to have obstructive triple-vessel CAD. The number of patients with obstructive or non-obstructive CAD for each coronary artery is detailed in Table 2. In addition, 80 of 86 patients had received a clinical echocardiogram as part of their standard of care. Among the 86 included patients, 53 were scanned with diverging wave compounding and 33 with ECG-gated focused acquisitions.

Strain imaging

In Figure 2 are left-ventricular, end-systolic axial, lateral, radial and circumferential strains in a normal patient, a patient with non-obstructive CAD and a patient with obstructive CAD. In a normal heart, positive axial strain is expected to be observed in the anterior and inferior regions, while positive lateral strains are expected to be observed in the septal and lateral regions. On the other hand, positive radial strains and negative circumferential strains are expected to be observed in all regions. In the patient with no CAD (Fig. 2A), positive radial strains in *red* is observed throughout the myocardium, indicating normal radial thickening. Circumferential strains are negative in all segments, except the

Table 2. Clinical characteristics of the 86 patients*

	Normal (n = 21, 24.4%)	Non-significant (n = 28, 32.6%)	Significant (n = 37, 43.0%)	*P* Value
Age (y)	62.3 ± 15.2	66.8 ± 9.8	69.8 ± 13.1	0.108
Body mass index (kg/m^2)	26.5 ± 4.6	26.7 ± 4.9	25.6 ± 4.1	0.596
Men, n (%)	7 (33.3%)	15 (53.6%)	29 (78.4%)	**0.003**
Hypertension, n (%)	11 (52.4%)	16 (57.1%)	30 (81.1%)	**0.039**
Diabetes, n (%)	9 (42.9%)	15 (53.6%)	17 (45.9%)	0.325
Smoker, n (%)	11 (30.1%)	4 (26.7%)	9 (60.0%)	0.730
Hyperlipidemia, n (%)	9 (42.9%)	14 (50.0%)	28 (75.7%)	**0.024**
CKD, n (%)	3 (14.3%)	4 (14.3%)	10 (27.0%)	0.340
COPD, n (%)	2 (9.5%)	1 (3.6%)	0 (0.0%)	0.165
WMAs, n (%)	0 (0%)	7 (26.9%)	8 (23.5%)	**0.0436**
No WMAs, n (%)	20 (100%)	19 (73.1%)	26 (76.5)	
Coronary disease, n				
LAD	0	26	27	
LCX	0	22	15	
RCA	0	23	18	

* Normal, non-obstructive and obstructive groups correspond to patients with highest stenosis level of 0%, 10%−49% and ≥50% stenosis in all coronary arteries combined.CKD = chronic kidney disease; COPD = chronic obstructive pulmonary disease; LAD = left anterior descending artery; LCX = left circumflex artery; RCA = right coronary artery; WMAs = wall motion abnormalities.

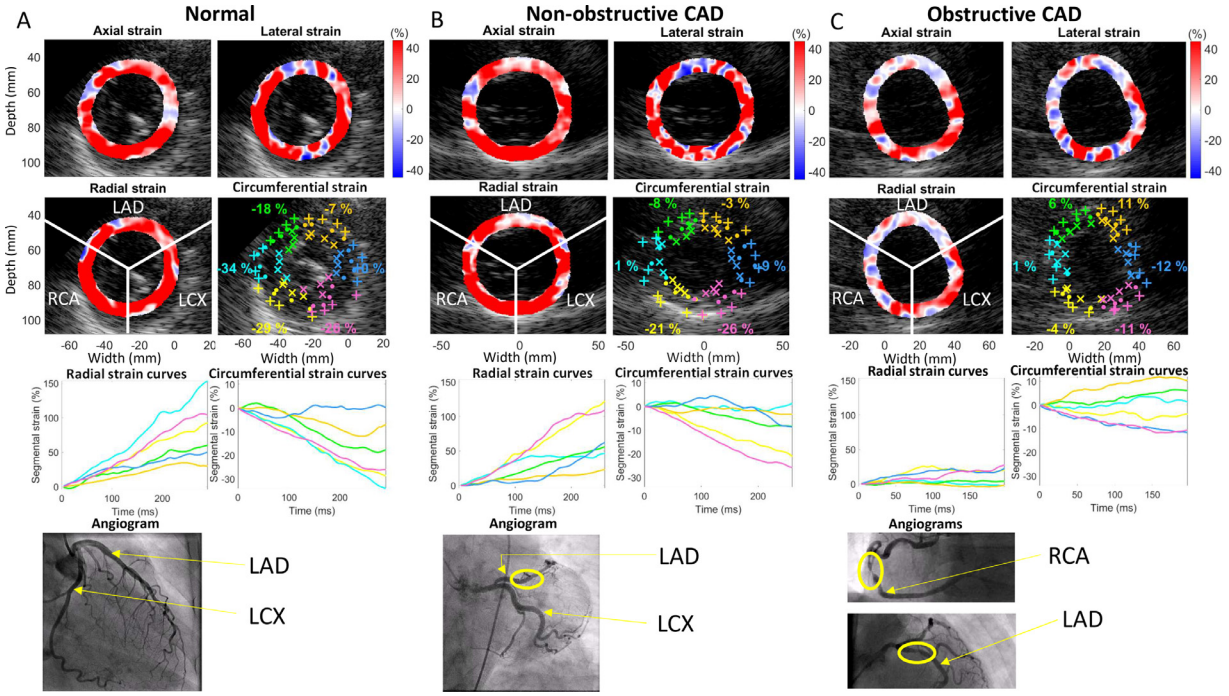

Fig. 2. Left ventricular, end-systolic axial, lateral, radial and circumferential strains in a normal patient (A), a non-obstructive CAD patient (30% stenosis in the proximal LAD) (B) and a obstructive CAD patient (60% stenosis in the proximal LAD, 40% stenosis in the proximal LCX, 70% stenosis in the proximal RCA and 90% stenosis in the midlevel RCA) (C). The LAD, LCX and RCA perfusion territories are delineated by the *white solid line*. End-systolic epicardial (+), myocardial (•) and endocardial (×) contours, as well as circumferential strain values in each AHA segment, are shown. Systolic segmental radial and circumferential strain curves are also shown. The corresponding angiogram for the normal, non-obstructive and obstructive patients are also shown. The *yellow circle* indicates the stenosis. CAD = coronary artery disease; ED = end diastole; ES = end systole; LAD = left anterior descending artery; LCX = left circumflex artery; LV = left ventricular; LAD = left anterior descending artery; LCX = left circumflex artery; RCA = right coronary artery.

lateral one. The patient with non-obstructive CAD (Fig. 2B) has 30% stenosis in the proximal LAD, and positive radial strains are also observed throughout the myocardium, with lower radial strain magnitude in the anterior region and lower circumferential strain magnitude in the anterior–lateral region. The patient with obstructive CAD (Fig. 2C) has 60% stenosis in the proximal LAD, 40% stenosis in the proximal LCX, 70% stenosis in the proximal RCA and 90% stenosis in the middle RCA. In this patient, with double-vessel obstructive CAD, decreases in radial strain magnitude and also negative strains (indicating radial thinning) are observed in LAD and RCA territories. In addition, circumferential strain curves in the territories perfused by coronaries with significant stenosis (LAD and RCA) exhibit positive (corresponding to passive relaxation) or significantly reduced strains compared with the normal and obstructive cases.

Statistical analysis

Left-ventricular end-systolic radial (Fig. 3A) and circumferential (Fig. 3B) strains were compared in each perfusion territory and for all patient groups. RCA territories with obstructive lesions had significantly lower radial strains than normal RCA territories (55.3 ± 29.8% vs. 73.4 ± 30.4%, $p < 0.05$) and non-obstructive RCA territories (55.3 ± 29.8% vs. 72.5 ± 46.8%, $p < 0.05$). A non-significant difference in radial strains was found in the LAD and LCX territories, although a trend toward decreasing strain as a function of stenosis level was observed. However, when all territories were combined, we also found that territories with obstructive lesions had significantly lower radial strain compared with normal territories (35.4 ± 25.1% vs. 52.7 ± 32.7%, $p < 0.0001$) or non-obstructive territories (35.4 ± 25.1% vs. 46.3 ± 36.0%, $p < 0.05$).

The mean circumferential strain in each territory and in each group is negative. When comparing the mean circumferential strain between groups, the term *higher* (or *lower*) indicates "higher in absolute value" (or "lower in absolute value") for simplicity. LAD territories with obstructive lesions had significantly lower circumferential strain than normal LAD territories (−3.1 ± 7.5% vs. −6.9 ± 8.0%, $p < 0.05$) and non-obstructive

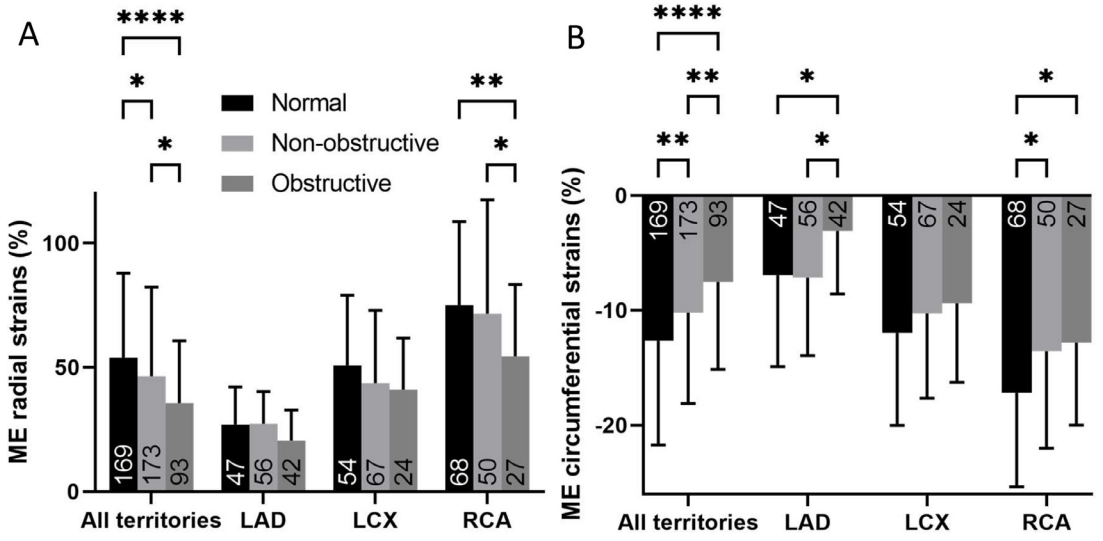

Fig. 3. Evolution of ME radial (A) and circumferential (B) strains with the degree of stenosis in each perfusion territory and in all territories combined. The number of territories in each group is indicated at the bottom of the corresponding bar. *$p < 0.05$, **$p < 0.01$, ****$p < 0.0001$. LAD = left anterior descending artery; LCX = left circumflex artery; ME = myocardial elastography; RCA = right coronary artery.

LAD territories (-3.1 ± 7.5 % vs. -7.2 ± 6.8%, $p < 0.05$). Normal RCA territories had significantly higher circumferential strain than obstructive RCA territories (-17.1 ± 8.2% vs. -12.8 ± 7.2%, $p < 0.05$) and non-obstructive RCA territories (-17.1 ± 8.2% vs. -13.6 ± 8.5%, $p < 0.05$). No significant difference in circumferential strains was found in the LCX territory, although a trend toward decreasing circumferential strain as a function of stenosis level was observed. When combining all territories, we also found that territories with obstructive lesions had significantly lower circumferential strain than normal territories (-7.5 ± 7.6% vs. -12.7 ± 9.1%, $p < 0.0001$) and non-obstructive territories (-7.5 ± 7.6% vs. -10.2 ± 7.9%, $p < 0.01$). Also, non-obstructive territories had lower circumferential strains than normal territories (-10.2 ± 7.9% vs. -12.7 ± 9.1%, $p < 0.01$). Axial displacements (and strains) are typically more accurate than lateral displacements because of the lack of phase information and coarser sampling in the lateral direction. Therefore, the accuracy of radial and circumferential strains, which depends both on the axial and lateral components, is not homogeneous. In particular, the anterior and posterior regions exhibit mainly overall axial motion, while the septal and lateral regions exhibit mainly lateral motion. This could partially explain the absence of statistical significance in strains in the different groups in the LCX territory, which depends significantly on lateral motion estimation.

A receiver operating characteristic (ROC) analysis was performed to assess the diagnostic ability of ME to classify patients based on their level of stenosis. Because ROC analysis is intended for binary classification and we have three groups, we performed two sets of ROC analysis in the LAD, LCX, RCA and all territories. In the first analysis, we attempted to classify the patient as having obstructive CAD versus not having obstructive CAD (normal coronaries and non-obstructive CAD) (Fig. 4A, B). In the second analysis, we attempted to classify the patient as having normal coronaries versus abnormal coronaries (non-obstructive and obstructive CAD) (Fig. 4C, D). The area under the ROC curve (AUC), sensitivity and specificity of the radial and circumferential ME strains in each territory and in all territories combined at the optimal cutoff value based on the Youden index are given in Table 3. When classifying patients as having obstructive CAD versus not having obstructive CAD, the AUC was higher in the LAD (0.65 for ME radial and 0.71 for ME circumferential strains) than in the RCA (0.64 for both ME radial and circumferential strains) and lower in the LCX (0.52 for ME radial and 0.56 for ME circumferential strains). When classifying patients as having normal coronaries versus abnormal coronaries, for radial strains the AUC was higher in the LAD (0.58) than in the RCA (0.57) and lower in the LCX (0.57), while for circumferential strains the AUC was higher in the RCA (0.67) than in the LAD (0.59) and lower in the LCX (0.57) (Table 4). On the other hand, when the normal group was compared with the group of non-obstructive and obstructive CAD, the sensitivity and specificity of WMAs were 25% and 100%, respectively. When comparing the group of normal and non-obstructive CAD against the obstructive CAD group, the sensitivity and specificity of WMA were 24% and 85%, respectively.

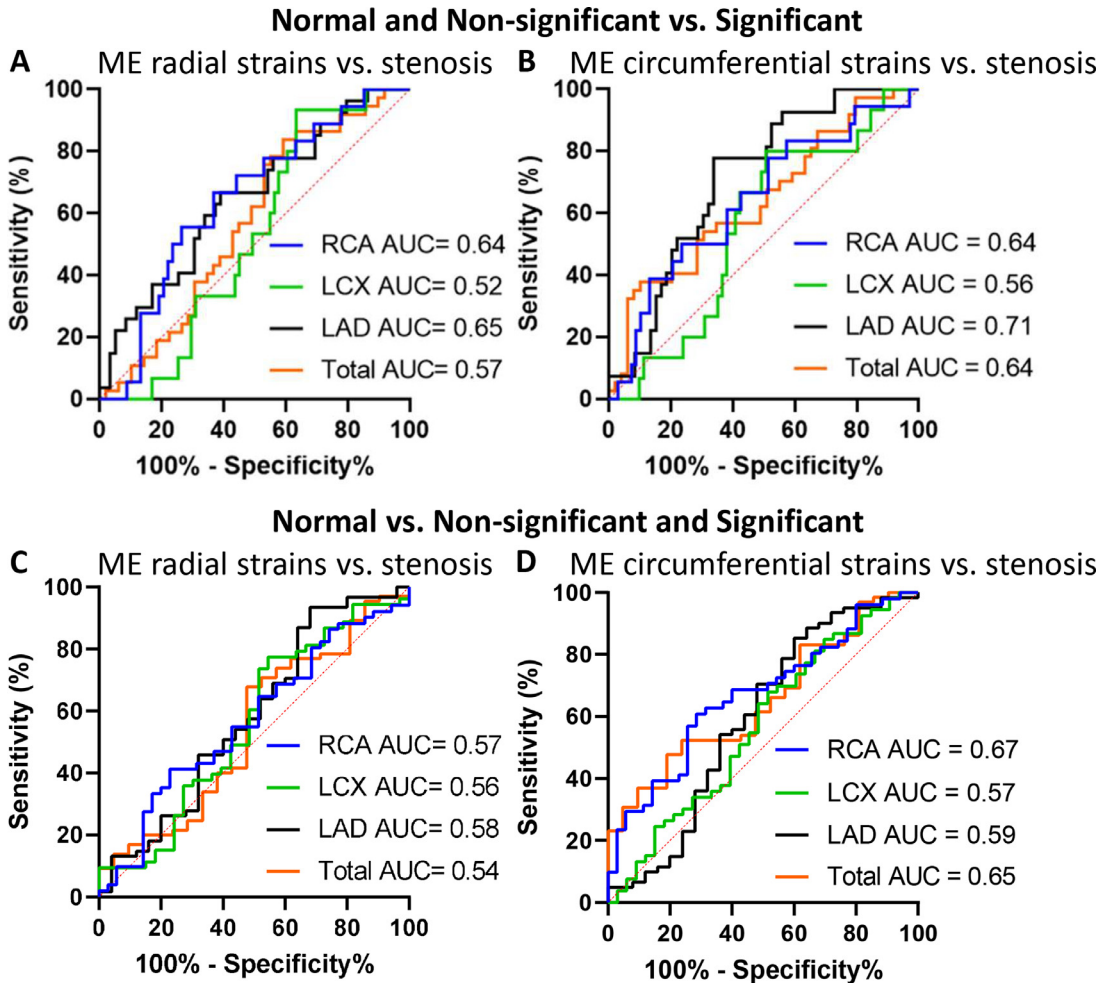

Fig. 4. Receiver operating characteristic curve for the diagnostic ability of ME to classify patients with obstructive stenosis versus those who do not have obstructive stenosis (A, B), as well as between patients with normal coronaries and those with abnormal (non-obstructive and obstructive) coronaries (C, D) in each territory and with all territories combined. AUC = area under curve; LAD = left anterior descending artery; LCX = left circumflex artery; ME = myocardial elastography; RCA = right coronary artery.

DISCUSSION

Non-invasive and radiation-free detection and characterization of CAD can assist in preventing normal patients from undergoing invasive procedures such as coronary angiography. It has been reported that almost 66% of patients referred for invasive coronary angiography with suspicion of CAD have normal or non-obstructive CAD (Patel et al. 2010). ME is an ultrasound technique that can image myocardial strains at high

Table 3. AUC, sensitivity and specificity of ME radial and circumferential strains to classify patient as having obstructive CAD versus non-obstructive CAD in each perfusion territory and all territories combined

	ME radial strains			ME circumferential strains		
	AUC	Sensitivity (%)	Specificity (%)	AUC	Sensitivity (%)	Specificity (%)
All territories	0.57	84	41	0.64	38	90
LAD	0.65	67	61	0.71	78	66
LCX	0.52	93	37	0.56	80	49
RCA	0.64	67	63	0.64	50	76

AUC = area under the receiver operating characteristic curve; LAD = left anterior descending artery; LCX = left circumflex artery; ME = myocardial elastography; RCA = right coronary artery.

Table 4. AUC, sensitivity and specificity of ME radial and circumferential strains used to classify patient as having normal coronary versus abnormal coronary stenosis in each perfusion territory and all territories combined

	ME radial strains			ME circumferential strains		
	AUC	Sensitivity (%)	Specificity (%)	AUC	Sensitivity (%)	Specificity (%)
All territories	0.54	68	52	0.65	48	81
LAD	0.58	93	32	0.59	85	40
LCX	0.56	77	45	0.57	68	48
RCA	0.57	41	77	0.67	61	71

AUC = area under the receiver operating characteristic curve; LAD = left anterior descending artery, LCX = left circumflex artery; ME = myocardial elastography; RCA = right coronary artery.

frame rates using the ultrasound RF signals. High-frame-rate imaging can be achieved using diverging wave imaging or ECG-gated acquisitions with focused transmission. Our objectives were to investigate the capability of ME radial and circumferential strains with compounding and ECG gating in differentiating normal, non-obstructive and obstructive coronary arteries.

Left-ventricular, end-systolic radial and circumferential strains were obtained in normal patients, patients with non-obstructive CAD and patients with obstructive CAD (Fig. 2). Patients with no CAD tended to have normal strains (Fig. 2A), while regions of reduced strain were observed in territories perfused by stenotic coronary arteries. For instance, ME radial strain in the patient with obstructive CAD in Figure 2C is reduced in the anterior, septal and inferior-septal regions, which is consistent with obstructive CAD in the LAD (60% proximal) and RCA (70% proximal, 90% middle) vessels. Regions of negative strain can result from the passive tethering caused by ischemia, as reported in previous studies (Holmes et al. 2005) and predicted by theoretical models (Lee et al. 2007). However, an obstructive stenosis is not necessarily hemodynamically significant. Indeed, it was reported that 65% of lesions with 50%−70% stenosis and one in five lesions with 70%−90% stenosis have normal fractional flow reserve (FFR $>$ 0.80) (Tonino et al. 2010). Therefore, normal function can also be observed in territories perfused by obstructive CAD vessels.

Figure 3 compares the left-ventricular, end-systolic radial (A) and circumferential (B) strains in normal patients and patients with CAD in each perfusion territory and with all territories combined. ME radial strains were capable of differentiating the obstructive CAD group from the non-obstructive CAD group and no CAD groups in the RCA territory. ME circumferential strains were capable of differentiating the obstructive CAD group from the non-obstructive CAD and normal groups in the LAD territory and to differentiate the normal group from the obstructive and non-obstructive CAD groups in the RCA territory. Although relatively high variability in ME strains were obtained in the different groups, their means were found to be significantly different. This could be due to the relatively large sample size of each group, especially when all territories are combined. Increasing precision and accuracy of strain estimates could reduce standard deviations in groups and further support the hypothesis that the observed differences are due to stenosis severity. ME circumferential strain performed better than ME radial strain in differentiating normal, non-obstructive and obstructive perfusion territories. When all perfusion territories were combined, both ME radial strain and ME circumferential strain were capable of differentiating each group (normal, non-obstructive and obstructive) from the other. This is of significant interest because previous studies reported that non-obstructive lesions can cause ischemia (Schuijf et al. 2006; Curzen et al. 2014; Park et al. 2015).

The ROC curves, indicating the sensitivity and specificity of ME strains to the anatomical significance of the stenosis (Fig. 4), indicate that the AUC for both radial and circumferential strains is higher in the LAD than in the RCA and lower in the LCX. The relatively low AUC, sensitivity and specificity can be due to relatively large variability (standard deviation) in strains in each group. Increasing ultrasound RF-based image and strain estimation quality can improve accuracy in patient classification. In this study, the sensitivity was found to be higher for ME than for WMAs. However, the specificity was found to be higher for WMAs than for ME. The low sensitivity of WMAs (24%−25%) may be due to the fact that the echocardiogram was performed at rest. Diagnosis of CAD with WMAs with echocardiography is usually performed during stress and has a sensitivity of 85% (Knuuti et al. 2018). This could provide a role for ME, which is typically used at rest and could enhance the sensitivity of echocardiography at rest beyond what WMAs can currently provide.

This study has several limitations. There are differences in some patient characteristics between the different groups. The proportions of men, hypertensive patients and patients with hyperlipidemia are higher in the groups where the lesion is more significant. A significant proportion of the patients (94/180) were excluded

from ME analysis because of insufficient echocardiographic windows (75/94, caused by clutter noise or rib shadows) and poor tracking (19/94). More specifically, for compounding acquisitions, 40 of 52 (77%) and 12 of 52 (23%) patients were excluded because of poor B-mode and poor tracking quality, respectively. For ECG-gated acquisitions, 35 of 42 (83%) and 7 of 42 (17%) patients were excluded because of poor B-mode and poor tracking quality, respectively. The proportion of patients excluded in our study is larger than usually reported in the literature, such as in Skaarup et al. (2021), where 21% of the patients were excluded from global circumferential strain analysis because of inadequate image quality. One of the reasons for a higher exclusion rate in our study can be the use of high-frame-rate imaging sequences, which favors temporal over spatial resolution as well a non-clinical ultrasound system, for which B-mode image quality is not as good as in clinical ultrasound scanners. In addition, the global mean strain (*i.e.,* the average strain across all segments for a given patient) were not computed because for a given patient, some segments were excluded from the analysis because of poor B-mode or tracking quality. Therefore, the global mean strain may be biased toward certain territories, which would make interpretation of the results difficult. Improvement in image quality while preserving the phase of the RF signals at high frame rates is being investigated to improve the quality of ME estimates and preserve the initial number of recruited patients throughout the analysis. In addition, the use of two different methods of ultrasound acquisition with slightly different precisions, with ECG-gated acquisitions being approximately 13% more precise than compounding sequences (Sayseng et al. 2020), can be sufficient to affect the strain distribution in the different groups. In addition, the PRF could be set higher and adjusted for each patient based on the imaging depth to increase the imaging frame rate, which can lead to improved motion and strain estimates. However, higher temporal resolution is usually obtained at lower spatial resolution or composite acquisitions. Therefore, further investigation is needed to investigate the optimal imaging sequence and, in particular, the optimal trade-off between spatial and temporal resolution. Also, while the division of the myocardium into LAD, LCX and RCA territories was standardized, there is an interparticipant variability of coronary anatomy (Voigt et al., 2015), which makes it difficult to align the perfusion territories with the echocardiographic views and can affect the relationship between regional strain and coronary stenosis level.

Left-ventricular end-systolic radial strain characterizes systolic function of the heart, but the level of stenosis is an anatomical characteristic. Discrepancies have been found between LV functional aspects such as coronary flow rate and myocardial perfusion and anatomical characteristics (percentage of stenosis) determined by coronary angiography (White et al. 1984; Gaemperli et al. 2008; Meijboom et al. 2008; Tonino et al. 2010). Therefore, a stenosis greater than 50% will not always cause functional impairment, and LV function can be impaired for stenosis less than 50%. In our study, the functional significance of the stenosis was not determined. However, our study obtained results consistent with those of other studies, which reported that patients with CAD have lower radial (Xie et al. 2016) and longitudinal (Biering-Sorensen et al. 2014; Gaibazzi et al. 2014) strain than healthy subjects. Also, in this study, ME strain was obtained at rest. While other studies have found that strain or strain rate at rest can differentiate normal patients from patients with CAD (Liang et al. 2006; Choi et al. 2009; Montgomery et al. 2012; Gaibazzi et al. 2014; Mansour et al. 2018), cardiac strain assessment during stress is expected to better discriminate normal patients from patients with CAD (Pellikka et al. 2020). This is of particular interest as, during stress, higher frame rates are needed for accurate strain estimation ($>$85 frames/s at a heart rate $>$160 beats/min) (Rösner et al. 2015) and conventional imaging methods (40−60 frames/s) (Amzulescu et al. 2019) may not provide sufficient temporal resolution for speckle tracking while ME can achieve 100−300 frames/s. Ongoing studies are investigating the potential of ME to detect and characterize CAD during stress.

In this study, end-systolic strain was used because it was the quantity recommended by the EACVI/ASE/Industry Task Force to standardize deformation imaging (Voigt et al. 2015) and is commonly reported for cardiac strain imaging (Amzulescu et al. 2019). The interframe displacements were accumulated over an average systolic duration of 280 $\pm$ 36 ms across all acquisitions included in the analysis, and end-systolic strain was obtained without applying drift compensation. End-diastolic strain could convey additional information but this was beyond the scope of this study. In addition, longitudinal strain may improve CAD characterization and will be the topic of future investigations.

The number of patients (N = 86) analyzed in this study is not sufficiently high to draw robust conclusions. A study with a larger number of patients should be carried out to determine if these preliminary findings are confirmed and to better determine the relationship between ME strains and the severity of the stenosis. A comparison between our method and strain imaging with clinical scanners was not performed and will be investigated in a future study.

CONCLUSIONS

Myocardial elastography radial strains were capable of differentiating obstructive CAD group from non-obstructive CAD and no CAD groups in the RCA territory. ME circumferential strains were capable of differentiating the obstructive CAD group from non-obstructive CAD and normal groups in the LAD territory and of differentiating the normal group from the obstructive and non-obstructive CAD groups in the RCA territory. ME circumferential strain performed better than ME radial strain in differentiating normal, non-obstructive and obstructive perfusion territories. This study indicates that ME has the potential to serve as an important screening tool for non-invasive, radiation-free and early detection of CAD.

This study was supported by the National Institutes of Health (R01-EB006042). The authors thank Ormarys Castellanos, Sarah Myoung, Lorena Geilen and David Hargrove for screening the patients, as well as the Cardiac Catheterization Laboratory for their assistance.

Conflict of interest disclosure—The authors declare no conflicts of interest.

REFERENCES

Alam SK, Ophir J. On the use of envelope and RF signal decorrelation as tissue strain estimators. Ultrasound Med Biol 1997;23:1427–1433.

Amzulescu MS, De Craene M, Langet H, Pasquet A, Vancraeynest D, Pouleur AC, Vanoverschelde JL, Gerber BL. Myocardial strain imaging: Review of general principles, validation, and sources of discrepancies. Eur Heart J Cardiovasc Imaging 2019;20:605–619.

Behar V, Adam D, Lysyansky P, Friedman Z. The combined effect of nonlinear filtration and window size on the accuracy of tissue displacement estimation using detected echo signals. Ultrasonics 2004;41:743–753.

Biering-Sorensen T, Hoffmann S, Mogelvang R, Zeeberg Iversen A, Galatius S, Fritz-Hansen T, Bech J, Jensen JS. Myocardial strain analysis by 2-dimensional speckle tracking echocardiography improves diagnostics of coronary artery stenosis in stable angina pectoris. Circ Cardiovasc Imaging 2014;7:58–65.

Chen H, Shi H, Varghese T. Improvement of elastographic displacement estimation using a two-step cross-correlation method. Ultrasound Med Biol 2007;33:48–56.

Choi JO, Cho SW, Song YB, Cho SJ, Song BG, Lee SC, Park SW. Longitudinal 2D strain at rest predicts the presence of left main and three vessel coronary artery disease in patients without regional wall motion abnormality. Eur J Echocardiogr 2009;10:695–701.

Cikes M, Tong L, Sutherland GR, D'Hooge J. Ultrafast cardiac ultrasound imaging: Technical principles, applications, and clinical benefits. JACC Cardiovasc Imaging 2014;7:812–823.

Curzen N, Rana O, Nicholas Z, Golledge P, Zaman A, Oldroyd K, Hanratty C, Banning A, Wheatcroft S, Hobson A, Chitkara K, Hildick-Smith D, McKenzie D, Calver A, Dimitrov BD, Corbett S. Does routine pressure wire assessment influence management strategy at coronary angiography for diagnosis of chest pain? The RIPCORD study. Circ Cardiovasc Interv 2014;7:248–255.

Gaemperli O, Schepis T, Valenta I, Koepfli P, Husmann L, Scheffel H, Leschka S, Eberli FR, Luscher TF, Alkadhi H, Kaufmann PA. Functionally relevant coronary artery disease: Comparison of 64-section CT angiography with myocardial perfusion SPECT. Radiology 2008;248:414–423.

Gaibazzi N, Pigazzani F, Reverberi C, Porter TR. Rest global longitudinal 2D strain to detect coronary artery disease in patients undergoing stress echocardiography: A comparison with wall-motion and coronary flow reserve responses. Echo Res Pract 2014;1:61–70.

Grondin J, Wan E, Gambhir A, Garan H, Konofagou E. Intracardiac myocardial elastography in canines and humans in vivo. IEEE Trans Ultrason Ferroelectr Freq Control 2015;62:337–349.

Grondin J, Waase M, Gambhir A, Bunting E, Sayseng V, Konofagou EE. Evaluation of coronary artery disease using myocardial elastography with diverging wave imaging: Validation against myocardial perfusion imaging and coronary angiography. Ultrasound Med Biol 2017a;43:893–902.

Grondin J, Sayseng V, Konofagou EE. Cardiac strain imaging with coherent compounding of diverging waves. IEEE Trans Ultrason Ferroelectr Freq Control 2017b;64:1212–1222.

Hasegawa H, Kanai H. High-frame-rate echocardiography using diverging transmit beams and parallel receive beamforming. J Med Ultrason 2011;38:129–140.

Holmes JW, Borg TK, Covell JW. Structure and mechanics of healing myocardial infarcts. Annu Rev Biomed Eng 2005;7:223–253.

Knuuti J, Ballo H, Juarez-Orozco LE, Saraste A, Kolh P, Rutjes AWS, Jüni P, Windecker S, Bax JJ, Wijns W. The performance of non-invasive tests to rule-in and rule-out significant coronary artery stenosis in patients with stable angina: A meta-analysis focused on post-test disease probability. Eur Heart J 2018;39:3322–3330.

Konofagou E, Ophir J. A new elastographic method for estimation and imaging of lateral displacements, lateral strains, corrected axial strains and Poisson's ratios in tissues. Ultrasound Med Biol 1998;24:1183–1199.

Konofagou EE, D'Hooge J, Ophir J. Myocardial elastography—A feasibility study in vivo. Ultrasound Med Biol 2002;28:475–482.

Lee WN, Ingrassia CM, Fung-Kee-Fung SD, Costa KD, Holmes JW, Konofagou EE. Theoretical quality assessment of myocardial elastography with in vivo validation. IEEE Trans Ultrason Ferroelectr Freq Control 2007;54:2233–2245.

Lee WN, Qian Z, Tosti CL, Brown TR, Metaxas DN, Konofagou EE. Preliminary validation of angle-independent myocardial elastography using MR tagging in a clinical setting. Ultrasound Med Biol 2008;34:1980–1997.

Lee WN, Provost J, Fujikura K, Wang J, Konofagou EE. In vivo study of myocardial elastography under graded ischemia conditions. Phys Med Biol 2011;56:1155–1172.

Liang HY, Cauduro S, Pellikka P, Wang J, Urheim S, Yang EH, Rihal C, Belohlavek M, Khandheria B, Miller FA, Abraham TP. Usefulness of two-dimensional speckle strain for evaluation of left ventricular diastolic deformation in patients with coronary artery disease. Am J Cardiol 2006;98:1581–1586.

Luo J, Bai J, He P, Ying K. Axial strain calculation using a low-pass digital differentiator in ultrasound elastography. IEEE Trans Ultrason Ferroelectr Freq Control 2004;51:1119–1127.

Luo J, Konofagou E. A fast normalized cross-correlation calculation method for motion estimation. IEEE Trans Ultrason Ferroelectr Freq Control 2010;57:1347–1357.

Ma C, Varghese T. Comparison of cardiac displacement and strain imaging using ultrasound radiofrequency and envelope signals. Ultrasonics 2013;53:782–792.

Mansour MJ, AlJaroudi W, Hamoui O, Chaaban S, Chammas E. Multimodality imaging for evaluation of chest pain using strain analysis at rest and peak exercise. Echocardiography 2018;35:1157–1163.

Meijboom WB, Van Mieghem CA, van Pelt N, Weustink A, Pugliese F, Mollet NR, Boersma E, Regar E, van Geuns RJ, de Jaegere PJ, Serruys PW, Krestin GP, de Feyter PJ. Comprehensive assessment of coronary artery stenoses: Computed tomography coronary angiography versus conventional coronary angiography and correlation with fractional flow reserve in patients with stable angina. J Am Coll Cardiol 2008;52:636–643.

Montalescot G, Sechtem U, Achenbach S, Andreotti F, Arden C, Budaj A, Bugiardini R, Crea F, Cuisset T, Di Mario C, Ferreira JR, Gersh BJ, Gitt AK, Hulot JS, Marx N, Opie LH, Pfisterer M, Prescott E, Ruschitzka F, Sabate M, Senior R, Taggart DP, van der Wall EE, Vrints CJ, Zamorano JL, Baumgartner H, Bax JJ, Bueno H, Dean V,

Deaton C, Erol C, Fagard R, Ferrari R, Hasdai D, Hoes AW, Kirchhof P, Knuuti J, Kolh P, Lancellotti P, Linhart A, Nihoyannopoulos P, Piepoli MF, Ponikowski P, Sirnes PA, Tamargo JL, Tendera M, Torbicki A, Wijns W, Windecker S, Valgimigli M, Claeys MJ, Donner-Banzhoff N, Frank H, Funck-Brentano C, Gaemperli O, Gonzalez-Juanatey JR, Hamilos M, Husted S, James SK, Kervinen K, Kristensen SD, Maggioni AP, Pries AR, Romeo F, Ryden L, Simoons ML, Steg PG, Timmis A, Yildirir A. 2013 ESC guidelines on the management of stable coronary artery disease: The Task Force on the management of stable coronary artery disease of the European Society of Cardiology. Eur Heart J 2013;34:2949–3003.

Montgomery DE, Puthumana JJ, Fox JM, Ogunyankin KO. Global longitudinal strain aids the detection of non-obstructive coronary artery disease in the resting echocardiogram. Eur Heart J Cardiovasc Imaging 2012;13:579–587.

Park HB, Heo R, O Hartaigh B, Cho I, Gransar H, Nakazato R, Leipsic J, Mancini GB, Koo BK, Otake H, Budoff MJ, Berman DS, Erglis A, Chang HJ, Min JK. Atherosclerotic plaque characteristics by CT angiography identify coronary lesions that cause ischemia: A direct comparison to fractional flow reserve. JACC Cardiovasc Imaging 2015;8:1–10.

Patel MR, Peterson ED, Dai D, Brennan JM, Redberg RF, Anderson HV, Brindis RG, Douglas PS. Low diagnostic yield of elective coronary angiography. N Engl J Med 2010;362:886–895.

Pellikka PA, Arruda-Olson A, Chaudhry FA, Chen MH, Marshall JE, Porter TR, Sawada SG. Guidelines for performance, interpretation, and application of stress echocardiography in ischemic heart disease: From the American Society of Echocardiography. J Am Soc Echocardiogr 2020;33:1–41 e8.

Provost J, Nguyen VT, Legrand D, Okrasinski S, Costet A, Gambhir A, Garan H, Konofagou EE. Electromechanical wave imaging for arrhythmias. Phys Med Biol 2011;56:L1–L11.

Radico F, Zimarino M, Fulgenzi F, Ricci F, Di Nicola M, Jespersen L, Chang SM, Humphries KH, Marzilli M, De Caterina R. Determinants of long-term clinical outcomes in patients with angina but without obstructive coronary artery disease: A systematic review and meta-analysis. Eur Heart J 2018;39:2135–2146.

Rösner A, Barbosa D, Aarsæther E, Kjønås D, Schirmer H, D'Hooge J. The influence of frame rate on two-dimensional speckle-tracking strain measurements: A study on silico-simulated models and images recorded in patients. Eur Heart J Cardiovasc Imaging 2015;16:1137–1147.

Sayseng V, Grondin J, Konofagou EE. Optimization of transmit parameters in cardiac strain imaging with full and partial aperture coherent compounding. IEEE Trans Ultrason Ferroelectr Freq Control 2018;65:684–696.

Sayseng V, Grondin J, Weber RA, Konofagou E. A comparison between unfocused and focused transmit strategies in cardiac strain imaging. Phys Med Biol 2020;65 03nt01.

Schuijf JD, Wijns W, Jukema JW, Atsma DE, de Roos A, Lamb HJ, Stokkel MP, Dibbets-Schneider P, Decramer I, De Bondt P, van der Wall EE, Vanhoenacker PK, Bax JJ. Relationship between noninvasive coronary angiography with multi-slice computed tomography and myocardial perfusion imaging. J Am Coll Cardiol 2006;48:2508–2514.

Shimoni S, Gendelman G, Ayzenberg O, Smirin N, Lysyansky P, Edri O, Deutsch L, Caspi A, Friedman Z. Differential effects of coronary artery stenosis on myocardial function: the value of myocardial strain analysis for the detection of coronary artery disease. J Am Soc Echocardiogr 2011;24:748–757.

Skaarup KG, Lassen MCH, Johansen ND, Olsen FJ, Lind JN, Jørgensen PG, Jensen G, Schnohr P, Prescott E, Søgaard P, Møgelvang R, Biering-Sørensen T. Age- and sex-based normal values of layer-specific longitudinal and circumferential strain by speckle tracking echocardiography: The Copenhagen City Heart Study. Eur Heart J Cardiovasc Imaging 2021; jeab032.

Stankovic I, Putnikovic B, Cvjetan R, Milicevic P, Panic M, Kalezic-Radmili T, Mandaric T, Vidakovic R, Cvorovic V, Neskovic AN. Visual assessment vs. strain imaging for the detection of critical stenosis of the left anterior descending coronary artery in patients without a history of myocardial infarction. Eur Heart J Cardiovasc Imaging 2015;16:402–409.

Tonino PA, Fearon WF, De Bruyne B, Oldroyd KG, Leesar MA, Ver Lee PN, Maccarthy PA, Van't Veer M, Pijls NH. Angiographic versus functional severity of coronary artery stenoses in the FAME study fractional flow reserve versus angiography in multivessel evaluation. J Am Coll Cardiol 2010;55:2816–2821.

Tsai WC, Liu YW, Huang YY, Lin CC, Lee CH, Tsai LM. Diagnostic value of segmental longitudinal strain by automated function imaging in coronary artery disease without left ventricular dysfunction. J Am Soc Echocardiogr 2010;23:1183–1189.

Varghese T, Zagzebski JA, Rahko P, Breburda CS. Ultrasonic imaging of myocardial strain using cardiac elastography. Ultrason Imaging 2003;25:1–16.

Virani SS, Alonso A, Benjamin EJ, Bittencourt MS, Callaway CW, Carson AP, Chamberlain AM, Chang AR, Cheng S, Delling FN, Djousse L, Elkind MSV, Ferguson JF, Fornage M, Khan SS, Kissela BM, Knutson KL, Kwan TW, Lackland DT, Lewis TT, Lichtman JH, Longenecker CT, Loop MS, Lutsey PL, Martin SS, Matsushita K, Moran AE, Mussolino ME, Perak AM, Rosamond WD, Roth GA, Sampson UKA, Satou GM, Schroeder EB, Shah SH, Shay CM, Spartano NL, Stokes A, Tirschwell DL, VanWagner LB, Tsao CW. Heart Disease and Stroke Statistics—2020 Update: A report from the American Heart Association. Circulation 2020;141:e139–e596.

Voigt JU, Pedrizzetti G, Lysyansky P, Marwick TH, Houle H, Baumann R, Pedri S, Ito Y, Abe Y, Metz S, Song JH, Hamilton J, Sengupta PP, Kolias TJ, d'Hooge J, Aurigemma GP, Thomas JD, Badano LP. Definitions for a common standard for 2D speckle tracking echocardiography: consensus document of the EACVI/ASE/Industry Task Force to standardize deformation imaging. Eur Heart J Cardiovasc Imaging 2015;16:1–11.

Wang S, Lee WN, Provost J, Luo J, Konofagou EE. A composite high-frame-rate system for clinical cardiovascular imaging. IEEE Trans Ultrason Ferroelectr Freq Control 2008;55:2221–2233.

White CW, Wright CB, Doty DB, Hiratza LF, Eastham CL, Harrison DG, Marcus ML. Does visual interpretation of the coronary arteriogram predict the physiologic importance of a coronary stenosis?. N Engl J Med 1984;310:819–824.

Xie MY, Lv Q, Wang J, Yin JB. Assessment of myocardial segmental function with coronary artery stenosis in multi-vessel coronary disease patients with normal wall motion. Eur Rev Med Pharmacol Sci 2016;20:1582–1589.

Zervantonakis IK, Fung-Kee-Fung SD, Lee WN, Konofagou EE. A novel, view-independent method for strain mapping in myocardial elastography: Eliminating angle and centroid dependence. Phys Med Biol 2007;52:4063–4080.